Advances in Science and Technology Research Journal

Advances in Science and Technology Research Journal, 2026, 20(7), 546–556
https://doi.org/10.12913/22998624/218878
ISSN 2299-8624, License CC-BY 4.0

Received: 2025.12.02
Accepted: 2026.05.15
Published: 2026.06.01

Intergranular corrosion resistance of HR3C heat-resistant austenitic stainless steel after long-term aging at 700 °C temperature

Grzegorz Golański[1], Karina Jagielska-Wiaderek[1], Tomasz Dudziak[2*]

[1] Czestochowa University of Czestochowa, Department of Materials Engineering, Armii Krajowej 19, 42-200 Czestochowa, Poland
[2] Lukasiewicz Research Network - Krakow Institute of Technology, Zakopiańska 73, 30-418 Krakow, Poland
* Corresponding author's e-mail: tomasz.dudziak@kit.lukasiewicz.gov.pl

ABSTRACT

The paper presents the results of research on the intergranular corrosion resistance of austenitic steel HR3C after long-term isothermal ageing at the temperature of 700 °C and time up to 40 000 h. During ageing the precipitation of $M_{23}C_6$ carbides as well as sigma and Z phases was observed in the steel microstructure. The susceptibility of the steel to intergranular corrosion was assessed on the basis of the degree of sensitization (DOS) ratio. It has been proved that in the initial ageing period of up to around 1000 h, the HR3C steel shows increased susceptibility to sensitization, connected with the precipitation of $M_{23}C_6$ carbides (DOS = 68%). As the time of ageing increased, the process of desensitization proceeded, leading to a decrease in the value of DOS to around 0.20% after 40 000 h. It has been concluded that the precipitation of sigma phase does not cause sensitization of the steel to intergranular corrosion. The obtained results indicate that long-term ageing of HR3C steel at the elevated temperature does not have to lead to the growth of the susceptibility to intergranular corrosion, and can promote its desensitization.

Keywords: microstructure, steel, high temperature, HR3C, aging, degree of sensitization.

INTRODUCTION

The HR3C (25Cr-20Ni-Nb-N) steel belongs to a modern group of heat-resistant austenitic stainless steels intended for use as structural materials for high-temperature applications such as ultra-supercritical (USC) power plant (as superheater (SH) and re-heater (RH) tubes). The HR3C steel was developed on the basis of TP310H steel as a result of modification of the chemical composition by reducing C content and introducing Nb and N. Those modifications were applied to increase high-temperature creep resistance. The high alloyed HR3C steel in as received conditions is supplied in a solution treated condition characterized by excellent high temperature oxidation resistance (steam and air) and flue gas corrosion resistance due to its high Cr content [1].

Stabilized austenitic steels [2, 3] should in theory be resistant to the phenomenon of sensitization. However, what is observed in a metastable microstructure of austenitic steels during the service at elevated temperature is the precipitation of particles rich in chromium on the boundaries of grains – at first the $M_{23}C_6$ carbides, and for longer periods of time, the precipitates of sigma phase [4, 5]. The presence of numerous chromium-rich particles on the boundaries of grains can lead to sensitization and growth of the susceptibility to intergranular corrosion (IGC) [3, 6]. Moreover, the $M_{23}C_6$ carbides precipitated on the grain boundaries are mostly responsible for an increase in brittleness of these alloys [4, 7].

What is demanded of steel for power industry is not only creep resistance – stability of the structure and functional properties through at

least 150 000 h, but also corrosion resistance in the service environment. Exposure in power units at the temperature range of 500–750 °C can result in the occurrence of IGC. Sensitization of steel of the austenitic matrix and the increase in its susceptibility to IGC can lead to degraded structure and mechanical properties, and consequently to costly failures [8–12]. Ensuring safe service of elements and parts of power units requires knowledge of potential risks. The main mechanism of degradation of the microstructure of austenitic steels are the processes of precipitation of secondary phases and changes in their morphology. Hence the necessity to understand the influence of changes running in the microstructure not only on the change in mechanical properties, but also on the resistance to corrosion, including the susceptibility to sensitization and IGC resistance. The influence of microstructure degradation occurring during the service of HR3C steel on the change in mechanical properties has already been relatively well presented in literature, as in [4, 13, 14]. However, there is a lack of sufficient knowledge about IGC resistance of HR3C steel during long-term aging or service. The research carried out so far in this field covered either the susceptibility of the alloy itself to this type of corrosion [15], or the heat affected zone of this steel [16] after short-term aging (time up to 500 hrs) or after heat treatment in the temperature range of 600–800 °C and time of annealing up to 24 h [17]. Results of these tests clearly show that for short times of annealing the HR3C steel is susceptible to intergranular corrosion. However, there is no knowledge about the susceptibility of this steel (or the lack of that susceptibility) to intergranular corrosion for longer times that are similar to the actual service time. Therefore, the paper focuses on investigating and analyzing IGC resistance of HR3C steel after long term aging up to 40 000 h at 700 °C temperature.

MATERIAL AND METHODOLOGY

HR3C steel was used in this work, the samples were cut and taken from the pipe section with the following dimensions of 12.5 × 50.1 mm. The examined material was long-term aged in laboratory conditions for 40 000 h at the temperature of 700 °C. Chemical composition of HR3C steel is given in Table 1.

The analysis of the chemical composition of the tested steel was carried out using the Bruker Q4 Tasman spark spectrometer. The microstructural studies were performed on conventionally prepared metallographic specimens, etched with the reagent copper sulfate ($CuSO_4$), using a scanning electron microscope JEOL JSM 6610LV (SEM) using 20kV accelerated voltage, figures were captured using secondary electron imaging (SEI) detector and backscatter detector (BSE) for surface topography and to highlight compositional differences (atomic number contrast) and deeper, subsurface structures. The identification of the precipitates was carried out using the TITAN 80–300 transmission electron microscope (TEM). The specimens for TEM analyses, i.e. thin films, were prepared as a disc of 3 mm in diameter and approx. 100 μm in thickness electrolytically thinned to perforation using a solution of 20% perchloric acid ($HClO_4$) in ethanol at a temperature of approx. 30 °C and voltage of approx. 20 V. The identification of precipitates on thin films was performed by selective electron diffraction (SED). The microsection surfaces were oriented perpendicularly to the axis of the pipe sample. Observation and recording of the surface images of the specimens after the corrosion test was carried out using the Keyence VHX 7000 Digital Microscope. To assess the degree of sensitization of steel to intergranular corrosion, the Double Loop Electrochemical Potentiokinetic Reactivation method (DL-EPR) was used, which consisted in anodic polarization of samples in a corrosion solution to a passive state, and then cathodic polarization. Measurements of electrochemical polarization were carried out in a classical three-electrode system using the CHI 1030A potentiostat using the cyclic volttameprometry method. The tests were performed in 0.5M H_2SO_4 containing 0.01 MKSCN (Potassium thiocyanate) at ambient temperature. Prior to the (DL-EPR), the working electrodes were cathodically polarized for 5 minutes to dissolve

Table 1. Chemical compostion of HR3C steel, %mass

C	Si	Mn	P	S	Cr	Ni	Nb	N
0.10	0.40	0.74	0.018	0.001	24.80	22.10	0.30	0.25

the oxide layer formed on the surface, after which the open-circuit potential (EOCP) was measured for them, later the EOCP was stabilized, DL-EPR measurements were started, conducting anode polarization in the potential range from -0.4 V to 0.0 V at a speed of 1.5 $mV \cdot s^{-1}$ and then reversing the scanning direction, conducting cathode polarization from 0.0 V to -0.4 at the same scanning rate. The values of all electrode potentials were expressed in relation to the silver chloride electrode. From the plotted curves, the peak activation current density (i_a) from the anode loop and the peak reactivation current density (i_r) from the reactivation loop were read. The method of determining parameters i_r and i_a is presented schematically in Figure 1.

The degree of sensitization (DOS) of the HR3C stainless steel can be calculated with the following Equation 1:

$$DOS = \frac{i_r}{i_a} \times 100\% \quad (1)$$

where: i_a and i_r are the current densities of the activation peak and reactivation peak in the DL-EPR curve, respectively.

For each test piece, the measurements were taken at least three times, obtaining a series of repeated polarization curves. Before each measurement, the working electrode was prepared through mechanical cleaning using waterproof abrasive paper of various grit sizes, ending with grit size 2000. After the corrosion test, working electrodes were ultrasonically cleaned, then air-dried and investigated using optical microscope (OM) and SEM. The analysed material was classified into the 4 sensitivity groups in accordance to the work proposed by Cihal et. al. [18] in the past:

- < 2% (method sensitivity threshold) the sample is classified as unsensitized;
- 2–8% traces of sensitization;
- 8–30% weakly and medium sensitized;
- > 30% severely sensitized.

RESULTS AND DISCUSSION

Microstructure in as received condition and after aging

Steel HR3C in the as-received state is provided in a supersaturated metastable state. The effect of such heat treatment is a microstructure consisting of austenitic matrix with numerous annealing twins and primary precipitates (Figure 2a). The primary precipitates were mostly placed near the grain boundaries, but also inside the grains. In the microstructure of the examined steel in the as-received state, large primary precipitates of the MX type and the Z phase were observed [4, 5]. However, no occurrence of any particles was observed on the boundaries of grains.

Isothermal ageing of HR3C steel at the temperature of 700 °C contributed to the changes in metastable microstructure of the examined alloy. Its visible effect was the precipitation of numerous

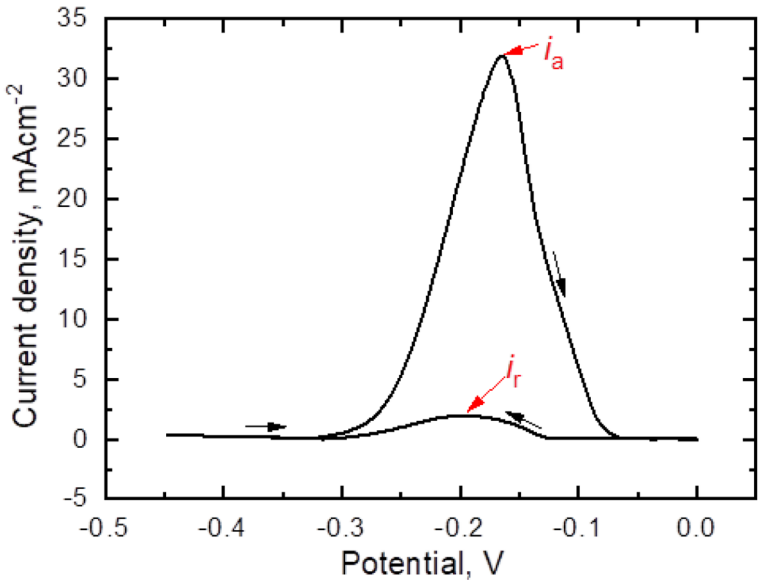

Figure 1. Establishing the values i_r and i_a from the polarization curves in this work

particles of secondary phases of diverse morphology (Figure 2b-2d). In the initial phase of ageing, the precipitation of chromium-rich $M_{23}C_6$ carbides could be observed on the boundaries of grains $M_{23}C_6$ (Figure 3, 4). Oversaturation of the matrix with chromium atoms and point defects results in the diffusing of chromium atoms or atom-vacancy complexes to areas of high energy, the grain boundaries, at the temperature of ageing. The preferential boundaries for nucleation and growth of $M_{23}C_6$ carbides in austenitic steels are defects of high degree of coincidence $\Sigma^3 9$ and high misorientation angle $\Theta > 45°$ [19, 20]. The solubility of carbon in the austenitic matrix, which is limited and changeable with the temperature, is a factor promoting fast precipitation of $M_{23}C_6$ carbides.

According to Jones et. al. [20], the precipitates of $M_{23}C_6$ carbides in austenitic steel 316 were observed already after one-hour ageing at the temperature of 600 °C. Further ageing contributed to an increase in the number of $M_{23}C_6$ carbides precipitated on the grain boundaries. The number of these particles was so large that they formed the so-called continuous grid of precipitates in some places (Figure 2b). Low thermal stability of $M_{23}C_6$ carbides translates into the coagulation of precipitates during ageing, which results in an increase in the particle size and widening of grain boundaries. According to Ostwald ripening mechanism, the growth of size of $M_{23}C_6$ particles with ageing time results in a decrease of their number density (Figure 2c and 2d). After longer times of annealing (above 5000 h of ageing), apart from the $M_{23}C_6$ carbides, a different precipitation in terms of morphology was observed at the grain boundaries – the chromium-rich sigma phase (Figure 2c, 2d, 5a). The susceptibility to the precipitation of sigma phase in austenitic steel can be evaluated using, inter alia, relation (2) [21] in the following form:

$$Cr_{eq} = Cr + 0.31Mn + 1.76Mo + \\ + 0.97W + 2.02V + 1.58Si + 2.40Ti + \\ + 1.17Nb + 1.22Ta - 0.226Ni - 0{,}177Co \quad (2)$$

In the case when the value of the chromium equivalent Cr_{eq} calculated from the Equation 2 amounts to over 17% mass, the steel is characterized by high tendency to the precipitation of sigma phase. In the case of the examined steel, the calculated value of Cr_{eq} amounted to 21.2%.

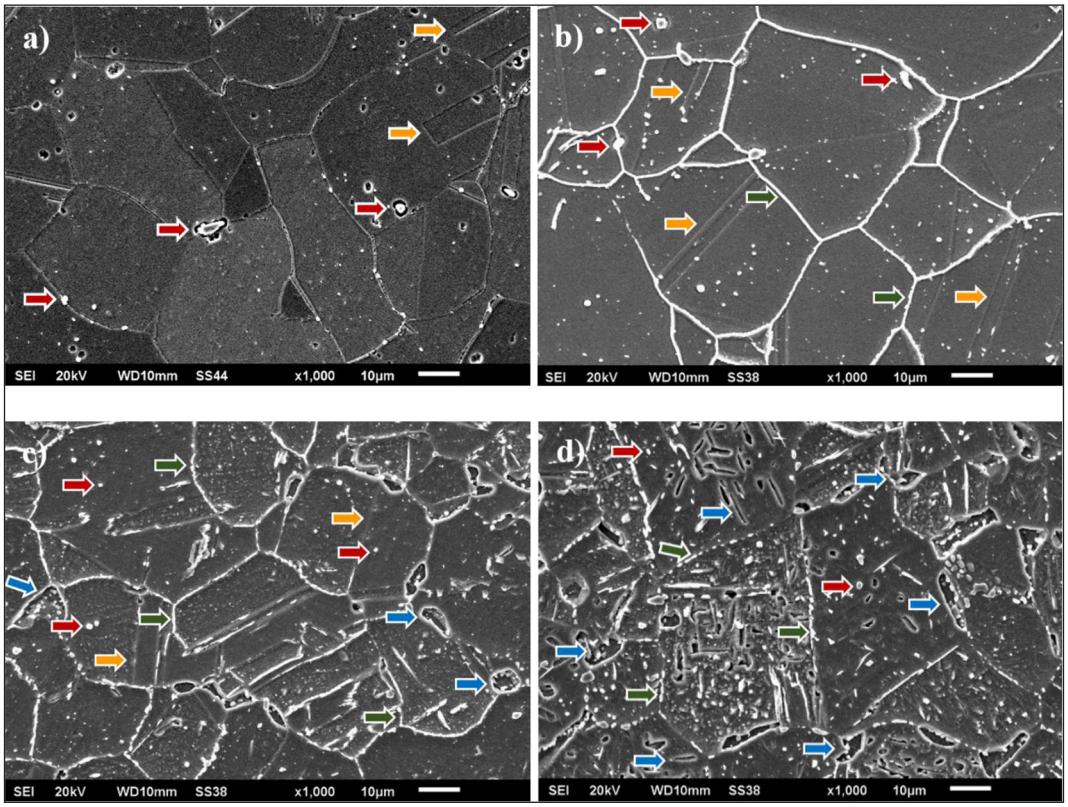

Figure 2. Microstructure of HR3C steel: (a) in as received condition; (b) after 100 h of ageing at 700 °C; c) after 5000 h of ageing at 700 °C; d) after 40 000 h of ageing at 700 °C; where: red arrows- primary particles; green arrows – M23C6 carbides; blue arrows – sigma phase; orange phase – twins

The formation of sigma phase is developing due to: 1. decomposition of delta ferrite; 2. independently of the matrix; 3. as a result of in situ transformation of $M_{23}C_6$ carbides [22, 23]. The sigma phase is facilitated by the high Cr content in a steel and the presence of strong carbide-forming elements (titanium, niobium) [22, 24]. The precipitation of sigma phase is promoted by high volume fraction of chromium in the steel and by the presence of highly carbide-forming elements (titanium, niobium) – limiting the volume fraction of carbon/nitrogen in the matrix [21, 24]. Silicon has a significant influence on accelerating the process of sigma phase precipitation in austenitic steels as well [25]. This effect is related to reduction of the precipitation activation energy of sigma phase [26]. During ageing, the process of enriching the sigma phase in silicon also takes place – Figure 6. The enrichment of the sigma phase in silicon is accompanied by its nickel and iron depletion [27]. Due to differences in diffusion rate of alloying elements (such as: Cr) and the redistribution of iron and chromium atoms [29], the precipitation of sigma phase in austenite is observed after several thousand hours. Initially the precipitates of sigma phase were visible mostly at the contact of three grain boundaries – the energetically privileged areas for the nucleation and growth of this phase (Figure 2c, 5). The precipitates of sigma phase were observed not only on the grain boundaries, but also inside the grains (Figure 5b). Inside the grains, apart

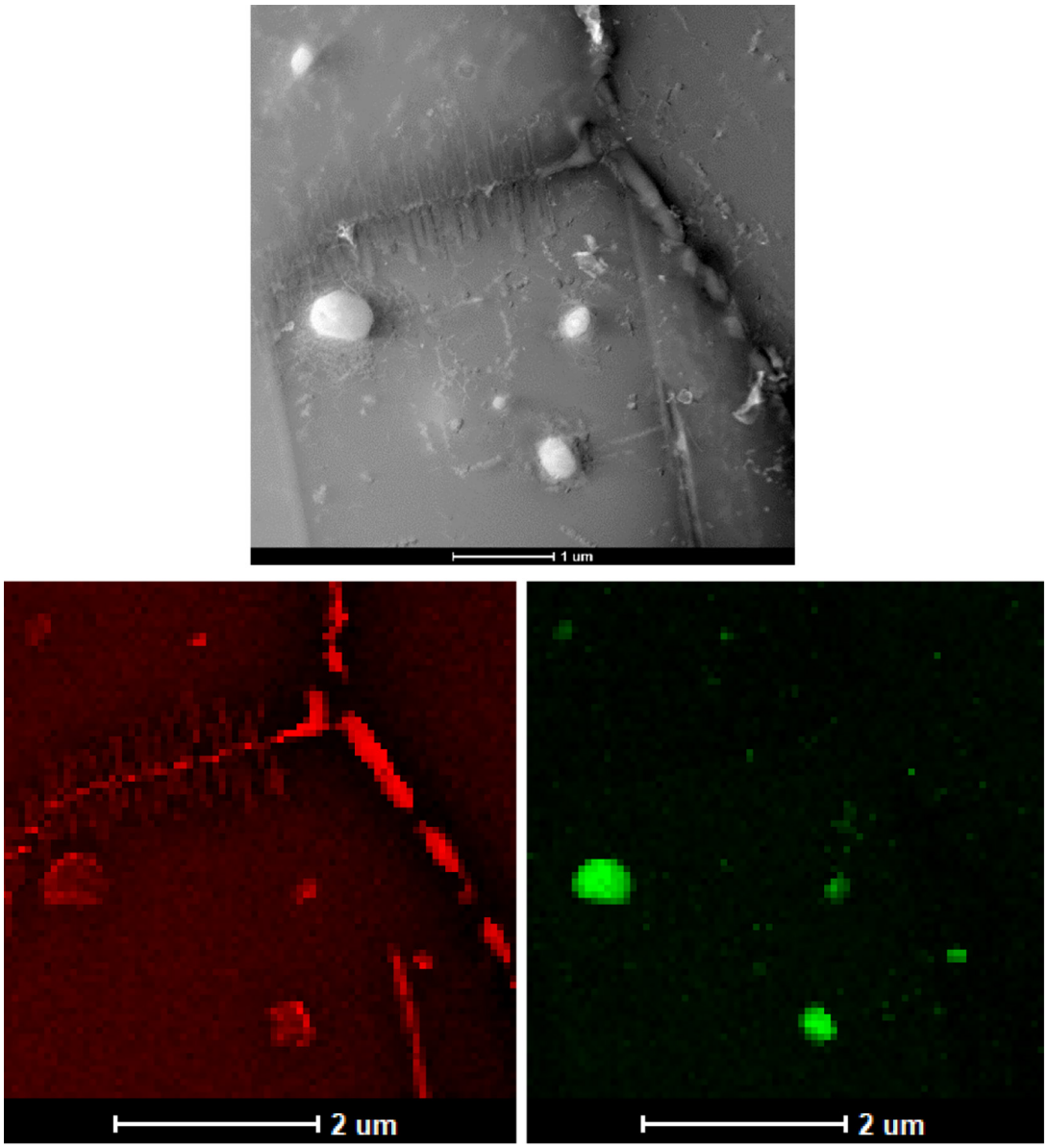

Figure 3. Microstructure of HR3C steel after aging process, SEM + EDS X-ray element distribution map

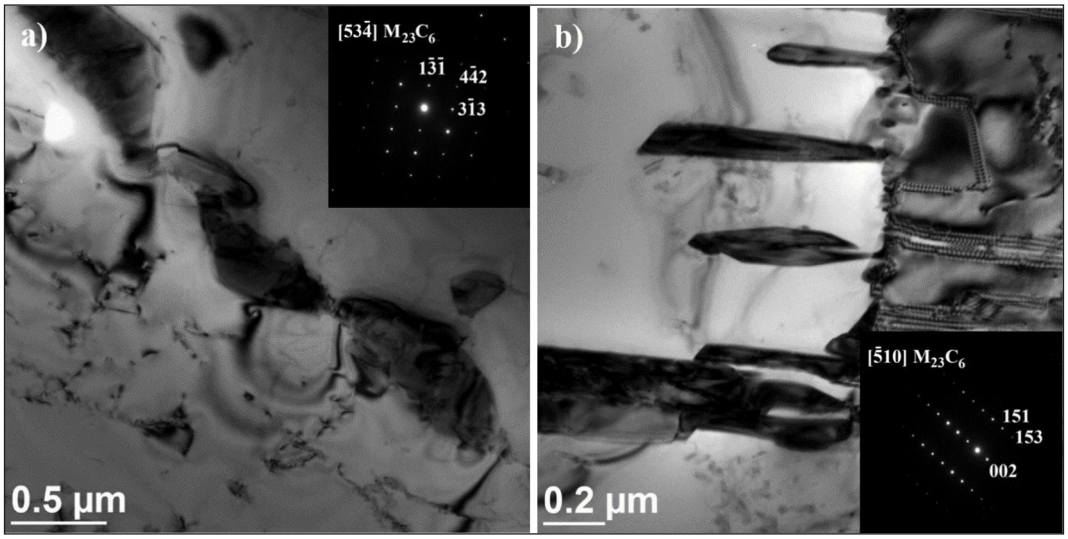

Figure 4. Precipitations of $M_{23}C_6$ carbides in HR3C steel after aging process: (a) at the grain boundary; (b) at twins

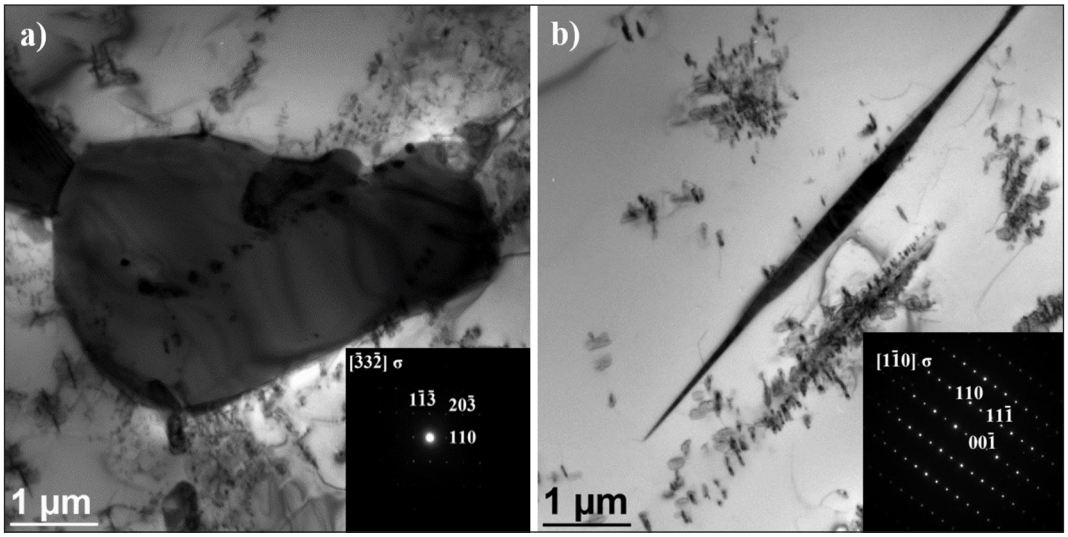

Figure 5. Precipitation of the sigma phase in HR3C steel after aging proces: (a) at grain boundaries triple junctions; (b) inside the grain

from the sigma phase precipitates, also the $M_{23}C_6$ carbides and the dispersive secondary precipitates of NbX and Z phase were revealed (Figure 7).

HR3C sensitization susceptibility

Austenitic steels in a supersaturated state (quickly cooled from the temperature of about 1050 ÷ 1150 °C) and heated/ operating at the temperature of 500 ÷ 800 °C are subjected to the phenomenon of sensitization. Sensitized austenitic steels are quite susceptible to intergranular corrosion (IGC) and intergranular stress corrosion cracking (ISCC) in chloride and caustic enviroments [28]. The susceptibility of austenitic steels to sensitization depends among other things on the chemical composition. The influence of chemical composition on the steel susceptibility to sensitization can be evaluated by determining the effective chromium content equation Cr^{eff} in the following form (3):

$$\begin{gathered} Cr^{eff} = Cr + 1.45Mo - 0.19Ni - \\ - 100C - 0.31Mn - 0.22Si - 0.51Al - \\ - 0.20Co + 0.01Cu + 0.61Ti + \\ + 0.34V - 0.22W - 9.2N \end{gathered} \tag{3}$$

Value Cr^{eff} (3) > 13.5 materials will have good resistance to IGC [28]. For the examined

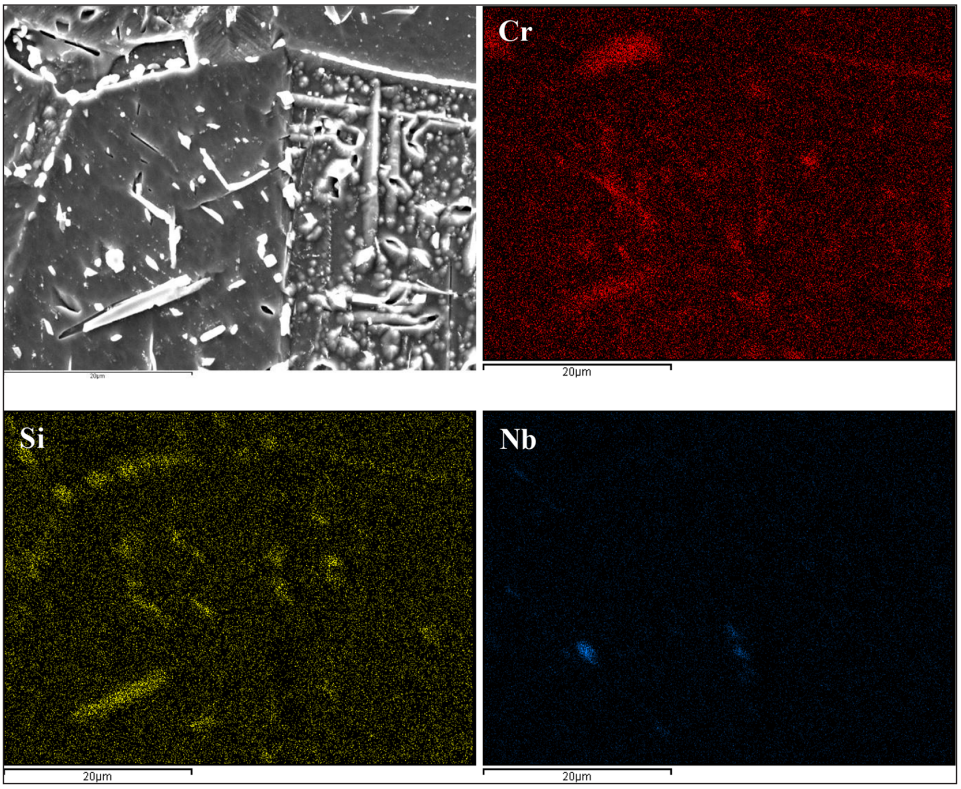

Figure 6. EDS X-ray map of the selected elements distribution in HR3C steel after 40 000 h of aging process at 700 °C

steel, the calculated value of Cr^{eff} (3) amounted to 12.91, which proves its susceptibility to intergranular corrosion.

It is known that the IGC in austenitic steels is connected with the precipitation of chromium-rich $M_{23}C_6$ carbides on the boundaries of grains. The precipitation of $M_{23}C_6$ carbides is related to short-range diffusion of carbon and chromium atoms from the matrix [20]. The differences in diffusion coefficients of atoms of these elements cause the carbon atoms to diffuse to the precipitating $M_{23}C_6$ carbides from the grain volume, whereas the chromium atoms from the near-boundary areas. This mean that the chromium consumption by the carbide-rich particles precipitationed at grain boundary cannot be supplemented in a timely manner by diffusion of chromium atoms from the grain. The results of this is forming Cr-depletion zones along grain boundaries. Decreasing the content of chromium below the critical value of 12% mass. results in preferential corrosion along the zones at grain boundaries due to the weakening of the passive layer in this area. It is known that higher chromium volume fraction in the steel ensures easier transition of the steel into the passive state, and therefore, the density of activation current has lower values (i_a). The value of current ia is connected with uniform dissolution of the entire surface of the material. After reversing the scanning direction of the potential, not the whole surface is subjected

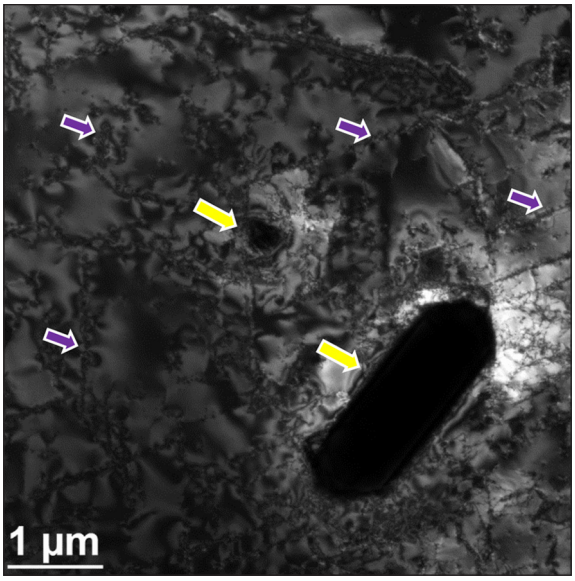

Figure 7. The primary precipitates (yellow arrows) and secondary precipitates (numerous purple arrows) in the HR3C austenitic steel matrix

Table 2. Values of current i_r and i_a, and DOS parameter

Heat tretment time [h]	i_r, [mA/cm^2]	i_a, [mA/cm^2]	DOS, [%]
0	0.05	16	0.31
100	9.60	14	68
1000	6.00	20	30
5000	1.50	25	6.00
10000	1.50	26	5.80
20 000	0.10	47	0.21
30 000	0.10	44	0.22
40 000	0.10	48	0.21

to dissolution, but the chromium-depleted areas, where the protective layer locally was with lower protective properties and reduced more easily. The higher the values of current density (ir) in this area, the more intense dissolution of the chromium-depleted grain boundaries is observed, therefore the higher the susceptibility of the material to intergranular corrosion occurs. It translates into the weakening of cohesion of the grain boundaries, and in consequence to grain fallout (Figure 8a). It significantly affects the behavior of alloy during the service in a corrosive environment, as well as its strength properties. Preferential grain boundary etching leads to microfractures, and as a result to a decrease in the resistance to cracking under mechanical loads [9, 11]. Consequently, the steel becomes more prone to damage in the service conditions.

Typical curves DL-EPR of the ageing for steel HR3C are shown in Figure 9, whereas Table 2 presents the determined values of ir and ia, and the value of DOS parameter calculated based on Equation 1.

The corrosion tests of aged HR3C steel showed that up to 1000 h of aging process initially significant increase in the DOS coefficient (68%) was observed asshown in Figure 9a, Figure 10. This value shows that the HR3C steel is susceptible to IGC process where dissolution of the grain boundaries takes place and loss of individual grains (as was shown in Figure 8a), leading further in loss of mechanical strength and oxidation resistance

Limited thermal stability of $M_{23}C_6$ carbides translates into the growth of their size and the formation of the so-called continuous grid of precipitates on the grain boundaries (Figure 2b, c). The carbide size growth is controlled by long-range diffusion of chromium atoms [7], however according to [4] this process depends on the grain boundary diffusion. Different volume fraction of chromium near the grain boundaries (Cr-depletion zone), compared to that inside the grain, causes concentration gradient, resulting in the diffusion of chromium atoms from the grain inside towards near-boundary areas. The result of this process is not only the coagulation of these particles [4], but also the progressive growth of chromium concentration in the depleted regions above the critical value. In effect the steel regains the corrosion resistance. Furthermore, according to [30], the

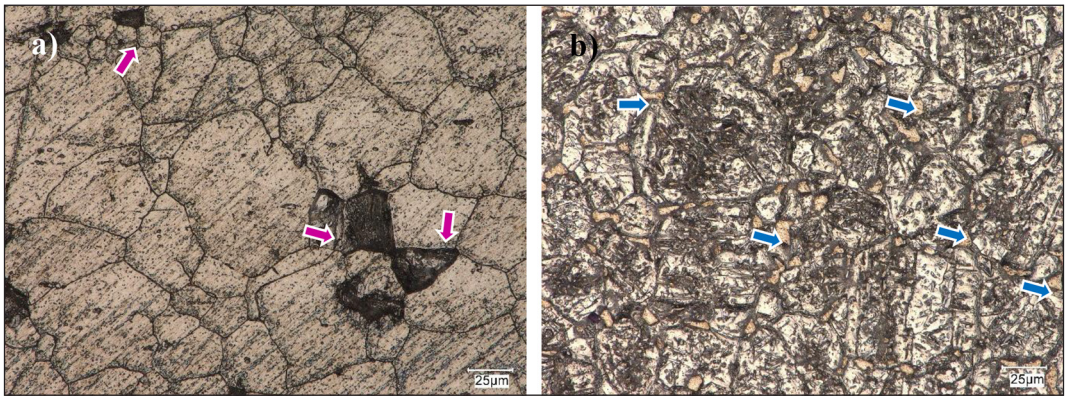

Figure 8. Microstructure of HR3C steel after test corrosion: (a) 100 h, (b) 40 000 h aged at 700 °C; magenta arrows – lack grain; blue arrows – sigma phase

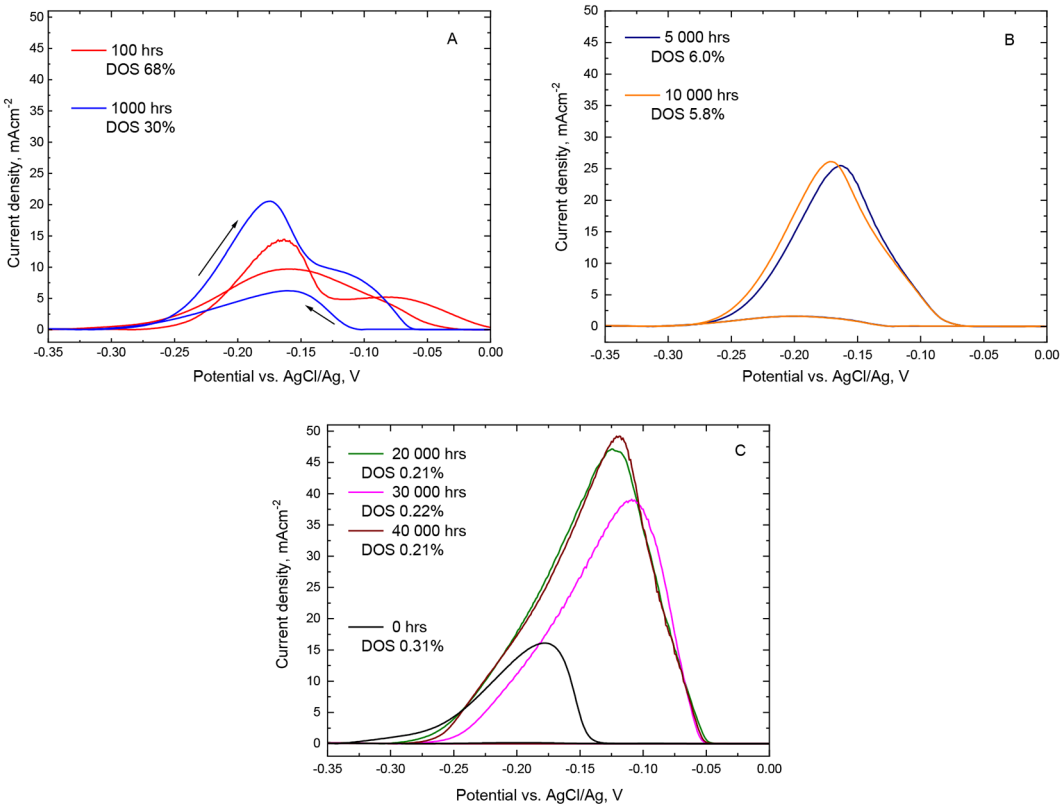

Figure 9. The DL-EPR curves and DOS values for the HR3C steel after various aging times at 700 °C

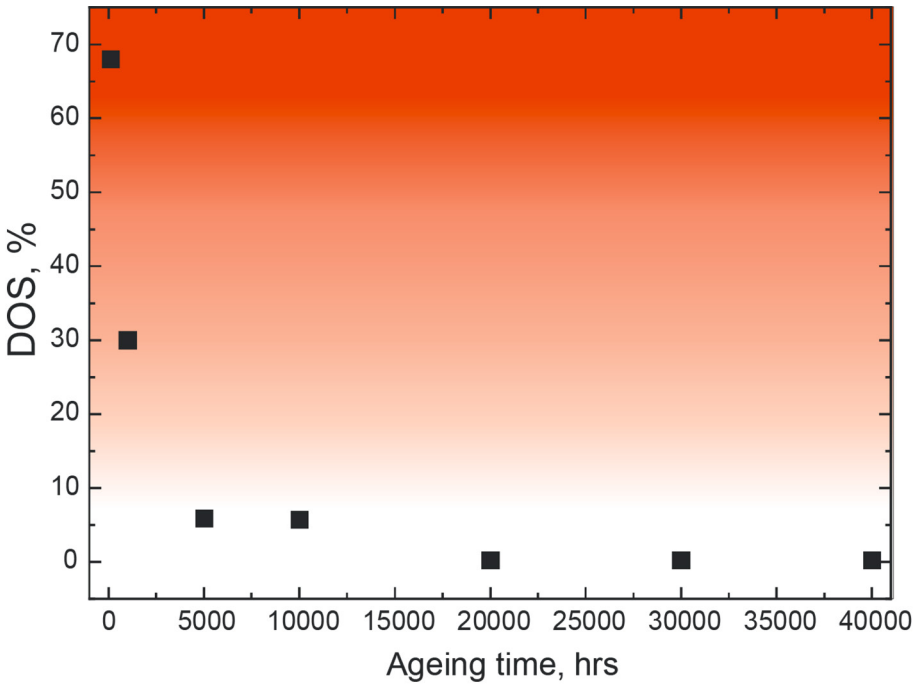

Figure 10. Change in DOS values with time under aging process at 700 °C for 40 000 h in HR3C steel

decrease of carbon concentration in the matrix as a result of the precipitation processes leads to a decrease in the activity of carbon, which can result in the increase of chromium content in the chromium-depleted zone near grain boundaries. The result of this phenomenon is a considerable reduction of the DOS parameter to around 6% (Figure 9b, 10). The occurrence of chromium-rich

precipitates of sigma phase in the microstructure or HR3C steel (Figure 2c, 2d, 5) does not contribute to the growth of sensitization of the analyzed alloy (Figure 8b, 8c, 9). The value of DOS parameter for structures containing precipitates of this phase ranges from 6.00% (for the ageing time of 5000 h) to 0.21% (for the ageing time of 40 000 h) – Figure 9c, 10. It was probably related to the following factors: 1. sigma phase is characterized by lower chromium volume fraction compared to $M_{23}C_6$ carbides; 2. the nucleation and growth of size of the sigma phase precipitates takes place at the expense of chromium-rich $M_{23}C_6$ carbides, which become the source of chromium atoms necessary for the nucleation and sigma phase growth; 3. the growth of sigma phase is mostly connected with the diffusion of chromium atoms along grain boundaries. According to, inter alia [22, 29], pre-existent chromium-rich particles in the austenitic stainless steel can be treated as precursors that intensify the formation of sigma phase. As shown in [30], after long-term service of austenitic TP321H steel above 200 000 h, in the microstructure on the grain boundaries, the $M_{23}C_6$ carbides are no longer observed, and only the particles of sigma phase and G phase forming a continuous grid can be seen. The value of DOS parameter for a given degree of microstructure degradation in the material was decreased to the value of around 0.2%, and for the time of ageing above 20000 h, a stable value of this parameter can be observed as a function of time (Table 2, Figure 9). The alloy becomes resistant to IGC, which is probably related to the leveling of chromium concentration between the near-boundary area and the inside of the grain. Similar mechanism of healing of an alloy during ageing was observed in austenitic steels as described in [3, 17]. Dynamic balance is created in the steel between the process of sensitization and desensitization. The presence of numerous $M_{23}C_6$ carbides, and sigma phase and Z phase particles rich in chromium in the microstructure of the aged steel (Figure 2) results in a decrease of the content of this element in the matrix. This results in a deterioration of the passivation ability of this alloy, since the critical passivation current (ia), which is a measure of the material ability to passivate easily, increases from the level of 16 $mAcm^{-2}$ for the as-received state to 48 $mAcm^{-2}$ for the material after 40 000 h of ageing (Figure 9c). Moreover, it is also important to mention that the quantitative growth of sigma phase in the microstructure of HR3C steel can contribute to the growth of the susceptibility of the alloy to pitting corrosion [31].

CONCLUSIONS

The austenitic steel HR3C was tested for the intergranular corrosion (IGC) resistance after long-term ageing at the temperature of 700 °C, and time up to 40 000 h, which reflects the material long-term service conditions at elevated temperature. At the initial stage of ageing, the HR3C steel showed increased susceptibility to intergranular corrosion, which is related to intense precipitation of numerous $M_{23}C_6$ carbides on the grain boundaries and local chromium-depletion of the matrix. Elongation of the ageing time in spite of the running microstructural changes resulted in the process of desensitization, leading to gradual regaining of the intergranular corrosion resistance by the HR3C steel. The occurrence of sigma phase precipitates in the analyzed steel structure does not cause a recurrence of the sensitization to intergranular corrosion. Precipitation of this phase mostly impacted the decrease in the resistance to general corrosion, which was reflected in the growth of anode current density i_a.

REFERENCES

1. Iseda A., Okada H., Semba H., Igarashi M., Long term creep properties and microstructure of SUPER304H, TP347HFG and HR3C for A-USC boilers, Energy Mater., 2007, 2, 199–206.
2. Dyja D., Rybarz M., Stradomski G., Januszka A., The role of stabilizing elemenyts in the ferritric welding wire in the microstrcutural and corrosion properties of the stainless steel weld joints, 8th European stainless steel&duplex stainless steel conference, Graz, Austria, 2015, 116–123.
3. Gajjar P. K., Khatri B. C., Siddhpura A. M., Siddhpura M. A., Sensitization and desenzitization (healing) in austenitic stainless steel: A critical review, Trans. Indian Inst. Met., 2022, 75, 1411–1427.
4. Zieliński A., Golański G., Sroka M., Evolution of microstructure and mechanical properties of HR3C austenitic stainless steel after ageing for up to 30000 h at 650–750 °C, Mater. Sc. Eng. 2020, 796A, 139944.
5. Zhao L., Li X., Xu L., Han Y., Hao K., Zheng X., Effect of microstructure evolution on mechanical properties and oxidation behavior of Super304H and HR3C aftrer long-term service, J. Mater. Sci., 2024,

59, 22206–22227.

6. Srinivasan N., Sensitization of autenitic stainless steels: Current developmnets, trends and future directions, Metall. Microst. Anal., 2021, 10, 133–147.
7. Wei L., Hao W., Cheng Y., Tan S., Isothermal aging embrittlement in an Fe-22Cr- 25Ni alloy, Mat. Sc. Eng. 2018, 737A, 40–46.
8. Golański G., Kolan C., Zieliński A., Klimaszewska K., Merda A., Sroka M., Kłosowicz J., Microstructure and mechanical properties of HR3C steel after service, Arch. Mater. Sc Eng., 2016, 81, 62–67.
9. Jung K.-H., Kim S.-J., Influence of sensitization on mechanical properties of AISI 304 stainless stell under high-temperature, J. Nanoscien. Nanotechn., 2019, 19, 4265–4269.
10. Xiao X., Li D., Li Y., Lu Sh., Intergranular precipitation behavior and its influence on the stress relaxation cracking susceptibility of Super 304H austenitic stainless steel weld metal during long-term aging, Mater. Charact., 2021, 178, 111309.
11. Bunchoo N., Wongpinkaew K., Kukiakulchai E., Kaekumsai S., Viyanit E., Effect of thermal history on sensitization behavior and Charpy impact property of type 316L and 316 stainless steels for applications in afired heater, Eng. Fail. Anal., 2022, 141, 106672.
12. Zhao L., Li X., Xu L., Han Y., Hao K., Zheng X., Effect of microstructure evolution on mechanical properties and oxidation behavior of Super304H and HR3C after long-term service, J. Mater. Sci., 2024, 59, 22206–22227.
13. Zhang J., Hu Z., Zhai G., Zhang Z., Gao Z., Creep damage characteristics and evolution of HR3C austenitic steel during long term creep, Mater. Sc. Eng., 2022, 832A, 142432.
14. Gao Z., Hu Z., Zhang J., Wang J., Zhang Z., Effect of on-service for 16000 and 38000 h on microstructure and mechanical properties of austenitic steel HR3C reheater tubes, Eng. Fail. Anal., 2023, 149, 107247.
15. Li X., Zhang Zh., Li Z., Zhou Y., Du B. Change of intergranular corrosion sensitivity of HR3C steel under the corrosion of 700 °C aging, IOP Conf. Series: Earth and Environmental Sc., 2019, 232, 022039.
16. Li X., Zhang Zh., Li Z., Du B., Li X., Wei Y., Research of intergranular corrosion of heat affected zone for HR3C steel after ageing treatment, IOP Conf. Series: Mater. Sc. And Eng., 2019, 569, 022023.
17. Du H., Cheng Y., Hou L., Li Y., We Y., Evolution of intergranular corrosion resistance for HR3C heat-resistant austenitic stainless steel at elevated temperature, Corr. Eng., Sc. Techn., 2017, 52, 343–348.
18. PN EN ISO 12732:2011 Corrosion of metals and alloys – Electrochemical potentiokinetic reactivation measurement using the double loop method (based on Cihal's method).
19. Wang X., Xu L., Jiao L., Li W., Mei J., Zhao Y., Qiao L., Inhibition of the intergranular brittleness of HR3C heat-resistant steel by strain-aging induced nano-$M_{23}C_6$ dispersion precipitation, JMRT, 2025, 213, 288–299.
20. Jones R., Randle V., Owen G., Carbide precipitation and grain boundary plane selection in overage type 316 austenitic stainless steel, Mat. Sci. Eng A., 2008, 496, 56–261.
21. Roychowdhury S., Kalin V., Matcheswala A., Bhandakkar A., σ-phase induced embrittlement in titanium containing austenitic stainless steel tie-bars in a condenser, Eng., Fail. Anal., 2012, 25, 123–132.
22. Barcik J., Mechanism of σ-phase precipitation in Cr-Ni austenitic steels, Mater. Sci. Tech., 1988, 4, 5–15.
23. Kishore K., Kushwaha S., Teja K. S. P., Chandan A. K., Mukherjee M., Adhikary M., Kumar A., Sigma phase embrittlement-induced failures nof heat-resistant stainless steel travelling grate links, Eng. Fail. Anal., 2023, 144, 106979.
24. Ren Q.-Q., Yamamoto Y., Brady M. P., Poplawsky J. D., Sigma phase evolution and nucleation mechanism revealed by atom probe tomography in a 347H stainless steel, Materialia, 2022, 24, 101485.
25. Lu Ch., Yi, H. Chen M., Xu Y., Wang M., Hao X., Liang T., Ma Y., Effect of Si on the stress rupture life and microstructure of a novel austenitic stainless steel, J. Mater. Sc. Techn., 2023, 25, 3408–3424.
26. Wang W.F., Wu M.J., Effect of silicon content and aging time on density, hardness, toughness, and corrosion resistance of sintered 303LSC-Si stainless steels, Mat. Sc. Eng. A. 2006, 425, 167–171
27. Padilha A.F., Rios P.R., Decomposition of austenite in austenite stainless steel, ISIJ Int., 2002, 42, 325–337.
28. Dayal R.K., Parvathavarthini N., Raj, B. Infleunce of metallurgical varaibles sensitization kinetics in austenitic steels, Inter. Mater. Rev. 2005, 50, 129–155.
29. Guan K., Xu X., Wang Z., Effect of aging at 700 °C on precipitation and toughness AISI 321 and and AISI 347 austenitic stainless steel welds, Nucl. Eng. Des., 2005, 235, 2485–2494.
30. Purzyńska H., Golański G., Zieliński A., Dobrzański J., Sroka M., Precipitation study in Ti-stabilised austenitic stainless steel after 207,000 h of service, Mater. A. T. High. Temp., 2019, 36, 296–303.
31. Silva D.D.S., Simoes T.A., Macedo D.A., Bueno A.H.S., Torres S.M., Gomes R.M., Microstructural influence of sigma phase on pitting corrosion behavior of duplex stainless steel/NaCl electrolyte couple, Mater. Chem. Phys., 2021, 259, 124056.